

Research Article

Open Access



Influence of Ca on the mechanical properties and microstructures of slag-fly ash geopolymers

Jing Li^{1,2}, Lang Yang^{1,2}, Feng Rao^{1,2}, Wenbiao Liu³, Hang Ma³, Xiaopeng Chi^{1,2}, Shuiping Zhong^{1,2}

¹Zijin School of Geology and Mining, Fuzhou University, Fuzhou 350108, Fujian, China.

²Fujian Provincial Key Laboratory of Green Extraction and Valuable Utilization of New Energy Metals, Fuzhou University, Fuzhou 350108, Fujian, China.

³R&D Center, Yunnan Yuntianhua Co., Ltd., Kunming 650228, Yunnan, China.

Correspondence to: Prof. Lang Yang, Zijin School of Geology and Mining, Fuzhou University, Wulong River North Avenue 2, Fuzhou 350108, Fujian, China. E-mail: siryanglang@foxmail.com; Prof. Feng Rao, Zijin School of Geology and Mining, Fuzhou University, Wulong River North Avenue 2, Fuzhou 350108, Fujian, China. E-mail: fengrao@fzu.edu.cn

How to cite this article: Li J, Yang L, Rao F, Liu W, Ma H, Chi X, Zhong S. Influence of Ca on the mechanical properties and microstructures of slag-fly ash geopolymers. *Miner Miner Mater* 2022;1:2. <https://dx.doi.org/10.20517/mmm.2021.02>

Received: 29 Nov 2021 **First Decision:** 6 Jan 2022 **Revised:** 16 Jan 2022 **Accepted:** 9 Feb 2022 **Published:** 24 Feb 2022

Academic Editors: Yanbai Shen, Feifei Jia **Copy Editor:** Xi-Jun Chen **Production Editor:** Xi-Jun Chen

Abstract

A deep understanding of the role of Ca in geopolymers exposed to various environments is essential for geopolymerization. This work evaluates the role of Ca by observing the behavior of hierarchically calciferous geopolymers under different environments including air, carbonization and freezing-thawing cycles. The structural and morphological differences between the geopolymers and the related mechanisms in various environmental conditions are assessed based on compressive strength, brunauer emmett teller, X-ray diffraction, fourier transform infrared spectroscopy, nuclear magnetic resonance spectroscopy and scanning electron microscopy measurements. It is found that two kinds of geopolymer gels, calcium silicate hydrate and sodium aluminosilicate hydrate, are formed in the geopolymerization of blast furnace slag and fly ash. Regardless of the specific air, carbonization or freezing-thawing cycle environment, the former gel dominates the properties in low Ca geopolymers, while the latter gel determines the properties in medium and high Ca geopolymers. Moreover, the carbonization environment enables calciferous geopolymers with higher surface areas and smaller pore sizes. Such adequate pore structures can significantly improve the performance of the geopolymers. This study presents novel insights into the influence of Ca on geopolymerization and in strengthening geopolymer properties.



© The Author(s) 2022. **Open Access** This article is licensed under a Creative Commons Attribution 4.0 International License (<https://creativecommons.org/licenses/by/4.0/>), which permits unrestricted use, sharing, adaptation, distribution and reproduction in any medium or format, for any purpose, even commercially, as long as you give appropriate credit to the original author(s) and the source, provide a link to the Creative Commons license, and indicate if changes were made.



Keywords: Blast furnace slag, fly ash, geopolymerization, compressive strength, microstructure

INTRODUCTION

Ordinary Portland cement (OPC) has been widely employed in civil engineering infrastructure projects. The production of OPC, however, requires significant energy consumption and limestone decomposition. About one ton of CO₂ may be discharged for the manufacturing of only one ton of OPC^[1], with global cement manufacturing releasing up to 4 billion tons of CO₂ every year^[2-4], representing up to ~8% of national CO₂ emissions^[5]. Energy constraints, global warming and intensifying public environmental consciousness have been growing sharply in numerous developing and developed regions. Thus, the use of alternative environmentally-friendly construction materials is being ever more investigated^[4]. Geopolymers represent green alternatives to OPC because they exhibit comparable mechanical properties and have much smaller energy consumption and significantly lower CO₂ emissions^[6-8]. Geopolymers are three-dimensional networks produced with many alumina- and silica-containing materials under highly alkaline conditions^[9]. It has been confirmed that geopolymers display superiority over OPC with regards to early strength growth and resistance against fire and chemical erosion^[10-12]. Therefore, geopolymers are regarded as promising alternatives to OPC. The most commonly employed starting materials to prepare geopolymers are clay and metakaolin, which are rich in alumina and silica^[13-15]. However, the most recent interest in geopolymers is for their utilization of industrial waste and by-products from the perspectives of waste circulation and resource conservation^[16-18].

The most readily available raw sources for geopolymers are fly ash (FA) and blast furnace slag (BFS), which are both aluminosilicates. FA is a waste produced by the combustion of coal in thermal power plants. Alumina and silica represent the essential components of FA, in addition to other impurities, including iron oxides and magnesia. BFS is a byproduct from the production of iron and mainly consists of silicon dioxide, calcium oxide, aluminum oxide and magnesium oxide. With rapid industrialization, FA and BFS waste has been produced in large quantities and has accumulated over years to become a significant threat to humans and the environment. The recycling of FA and BFS to prepare geopolymers not only has the potential to save natural aluminosilicate resources but also relieves the growing burden of FA and BFS on the environment. There have been numerous studies on the use of alkali-activated FA, BFS and FA-BFS materials to prepare geopolymers^[5,19,20]. To achieve practical compressive strength, a certain BFS is usually added to the FA. During the geopolymerization process, the Ca presented in BFS encounters hydration and generates calcium silicate hydrate gel (C-S-H), which is a cementitious phase that can improve its setting and strength performance^[21]. Many investigations have proved that the presence of BFS shortens the setting time and enhance the strength of geopolymers^[22,23]. However, even if FA-BFS geopolymers have practical strength, their short setting times of < 1 h, may lead to difficulties in their practical application in construction activities. Researchers have proposed that the influence of Ca ions should account for these geopolymers^[21].

Lloyd *et al.*^[24] and Temuujin *et al.*^[25] reported that Ca plays an essential role in the early strength development of geopolymers due to the formation of an intensified aluminosilicate gel. Moreover, Yip *et al.*^[26] found the coexistence of geopolymeric and C-S-H gels in the same metakaolin-slag geopolymer. Yip *et al.*^[27] also proposed that soluble Ca ions can greatly accelerate the hardening progress^[24], while Garcia-Lodeiro *et al.*^[28] reported the phase diagrams of CaO-SiO₂-Al₂O₃-Na₂O according to detailed solution/precipitation explorations. In addition, Khan *et al.*^[29] discovered that the types and proportions of reaction products in geopolymers depend on various factors, including alkalinity, ratios of aluminosilicate to calcium source and dissolution rates of alkali metal ions from aluminosilicate and calcium sources^[30,31].

Therefore, the interactions between calcium resources, silicate and aluminate are very complicated and the exact mechanisms require further exploration. The role of Ca also requires further verification in order to optimize the practical applications of geopolymers.

The present work uses environmentally-friendly alkali-activated high calcium BFS and FA to synthesize a series of functional geopolymers. We adjust the calcium content and C-S-H gel generation through the control of the BFS proportion in the geopolymers. We also explore the evolution and variation of the prepared geopolymers under different artificial natural environments, including air, carbonization and freezing-thawing cycles. The unique role of Ca in the general geopolymers is considered using X-ray diffraction (XRD), Fourier transform infrared (FT-IR) spectroscopy, nuclear magnetic resonance (NMR) spectroscopy, scanning electron microscopy (SEM) and compressive strength measurements.

EXPERIMENTAL

Materials

The raw FA and BFS were obtained from the Huaneng Fuzhou Power Plant in Fujian province and the Tangshan Iron and Steel Smelter in Hebei province, respectively. The particle size distributions of FA and BFS are presented in [Figure 1A](#), with d_{50} and d_{90} values for FA of 13.3 and 32.7 μm , and values of 7.2 and 17.6 μm for BFS, respectively. The components in FA and BFS are presented in [Table 1](#). FA mainly includes SiO_2 (45.47%) and Al_2O_3 (38.77%), while BFS mainly contains CaO (38.55%), SiO_2 (30.57%) and Al_2O_3 (15.09%).

The chemical composition and crystal structure of the FA and BFS are characterized in [Figure 1B](#). The FA shows many sharp peaks among the test range, which means that the components in FA possess good crystal structures and the peaks indicates that the components mainly consist of mullite [$\text{Al}_2(\text{Al}_{12.8}\text{Si}_{1.2})\text{O}_{9.54}$, PDF: 84-1205] and quartz (SiO_2 , PDF: 83-2465). As for the BFS, there is a wide amorphous peak at 2θ of 20-45°, which can be attributed to the peaks from calcite (CaCO_3 , PDF: 00-003-0596). Sodium silicate purchased from Aladdin Chemical Reagents was employed as an alkali activator to prepare the geopolymers. Deionized water was used throughout the whole process.

Methods

To prepare the geopolymer samples, a sodium silicate solution (6.17 mol/L) was employed as an activation solution and mixed with the starting materials for 10 min. The starting materials consisted of 30 g of a FA and BFS mixture, in which the BFS proportion changed from 20% to 100%. Subsequently, the mixture was put into designed cubic steel molds (30 mm × 30 mm × 30 mm) and the molds were vibrated on vibration tables for 3 min to remove the air bubbles in the mixture. After that, the molds were sealed inside plastic bags and cured under 60 °C for 6 h and left under 25 °C (room temperature) for seven days to finish the hydration progress and obtain original geopolymers. Finally, the original geopolymers were exposed to three typical simulated natural environments for 14 days in: (1) air; (2) a carbonized environment (temperature ± 20 °C, humidity ± 70% and concentration ± 20%); and (3) heat-cool seawater cycles. The geopolymers were also exposed to a freezing-thawing machine (4 to -18 °C, cycle time 4 h).

Measurements

The particle size was detected using a laser diffraction analyzer (LS-CWM, Omec, China). The components in FA and BFS were measured with an X-ray fluorescence instrument (Axios Advanced, The Netherlands). The chemical composition and crystal structure of FA and BFS were characterized with XRD (D8, Bruker, Germany). The compressive strength of the geopolymers was analyzed by a YAW-300 compression and flexure machine from Jinan Tianchen Manufacturing (Jinan, China). The microstructure of the mortars was characterized by SEM (JEM-2100 F, China) and NMR spectroscopy (Bruker AVANCE III, China). The BET

Table 1. Main components in FA and BFS

Component (%)	SiO ₂	Al ₂ O ₃	CaO	Fe ₂ O ₃	MgO	TiO ₂	Na ₂ O	K ₂ O
FA	45.47	38.77	5.11	4.08	1.90	1.41	0.73	1.04
BFS	30.57	15.09	38.55	0.33	1.305	1.60	0.50	0.37

FA: Fly ash; BFS: blast furnace slag.

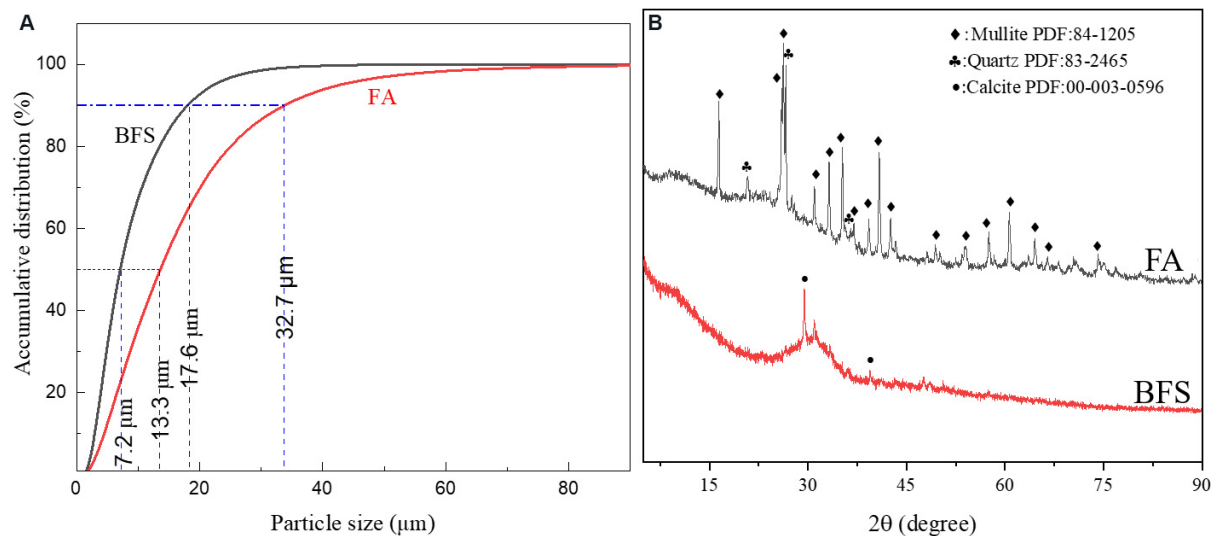


Figure 1. (A) Particle size distributions and (B) XRD patterns of FA and BFS. XRD: X-ray diffraction; FA: fly ash; BFS: blast furnace slag.

surface area and pore properties of the samples were acquired by N₂ adsorption/desorption isotherms and the Barrett-Joyner-Halenda method (Micromeritics ASAP2460). FT-IR spectra were collected using an FT-IR spectrometer (Vector-22, Bruker, Germany).

RESULTS AND DISCUSSION

Compressive strength

The compressive strength of the geopolymers prepared with different proportions of BFS at different exposure conditions are presented in [Figure 2](#). When exposed to air, carbonization and freezing and thawing environments, the compressive strength of the geopolymers with 20% and 50% BFS are 11.7, 12.5 and 7.5 MPa and 11.3, 11.7 and 6.7 MPa, respectively. Obviously, the compressive strength of the geopolymers in the three conditions exhibits various degrees of attenuation when the BFS proportion increases from 20% to 50%. The results can be attributed to the cracks in the test block caused by the evaporation of water. At the same BFS proportion, 20% or 50%, the geopolymer exposed in carbonization obtains the highest compressive strength, next is the geopolymer exposed in air and the geopolymer in freezing and thawing displays the lowest performance. In the carbonization environment, CaCO₃ is generated by the reaction of CO₂ with the C-S-H gel and Ca(OH)₂ to fill the pores in the system due to water evaporation, making the compressive strength slightly higher than that in the air. The freezing and thawing process may certainly hinder the geopolymerization and destroy the geopolymer structure, thereby resulting in poor compressive strength. Furthermore, the geopolymer prepared with the 100% BFS freezing-thawing system exhibits the most severe deterioration, which failed to be subjected to a compressive strength measurement.

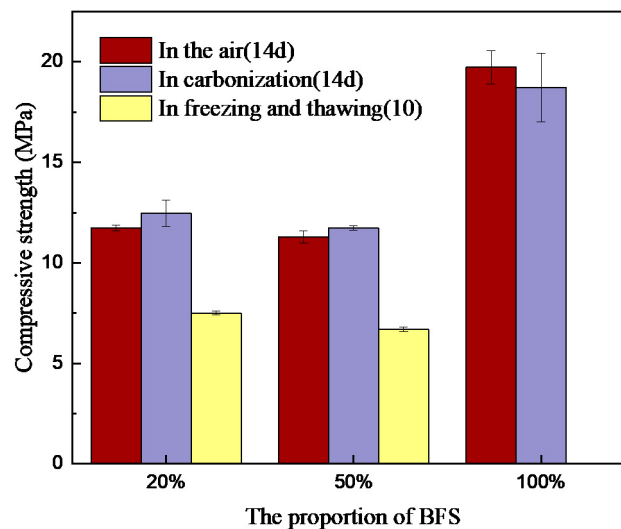


Figure 2. Compressive strength of geopolymers prepared with different proportions of BFS in air, carbonization and freezing-thawing process. BFS: Blast furnace slag.

As the BFS proportion increases to 100%, the compressive strength of the geopolymer in air and carbonization increases to 19.7 and 18.7 MPa, respectively, which are much higher than those of 20% and 50%. This may be caused by the more calcium sources in BFS, thus offering more precursors and generating more cementitious gel in the geopolymer with a higher content of BFS. It is noteworthy that the geopolymer with 100% BFS in air performs higher compressive strength than that in the carbonization environment, which is different from the geopolymers with 20% and 50% BFS. The reason is that too much CaCO_3 generated in the geopolymer when exposed to the carbonization environment, resulting in the decrease of alkali concentration in the pores and increase of the expansion material, leading to internal cracking and then the loss of compressive strength.

Microstructural characterization

XRD analysis

Figure 3 presents the XRD patterns of the geopolymers prepared with different proportions of BFS in the exposure conditions of air, carbonization and freezing-thawing cycles. Figure 3A shows the XRD of geopolymers exposed in air. The results indicate that the original quartz phase and mullite crystal from FA and the calcite phase from BFS could be obviously observed. Meanwhile, two new peaks at 29.6° and 49.7° related to the C-S-H gel occur, indicative of the geopolymerization reaction^[32]. With the addition of BFS from 20% to 50%, the characteristic peaks of FA continuously decrease, while the peaks of the C-S-H gel increase. For the geopolymers exposed to carbonization [Figure 3B] and freezing-thawing cycles [Figure 3C], their XRD patterns exhibited similar trends, indicating that the formation process of the geopolymers was slightly effected by the exposure environments, and the C-S-H generation can obviously improve the performance of the geopolymers. Thus, we can speculate that the formation rate of C-S-H is fast and a large amount of C-S-H gel can be generated at the initial stage of the geopolymer reaction, which accelerates the dissolution of Si and Al from FA and BFS. In addition, C-S-H can act as a condensation core to accelerate the formation of N-A-S-H and make the gel structure more compact, which is consistent with the results of higher compressive strength.

FTIR analysis

The FTIR spectra of the geopolymers prepared with different proportions of BFS in different exposure

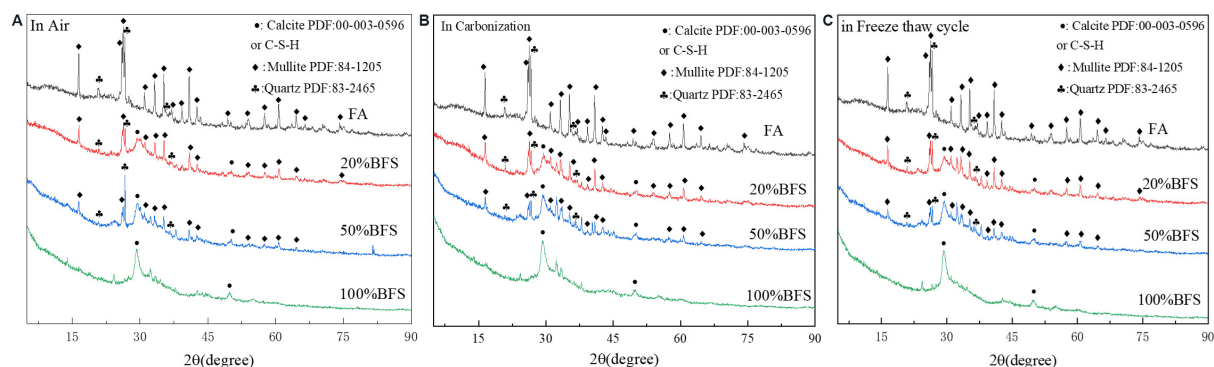


Figure 3. XRD patterns of geopolymers prepared with different proportions of BFS in (A) air, (B) carbonization and (C) freezing-thawing process. XRD: X-ray diffraction; BFS: blast furnace slag.

conditions are illustrated in [Figure 4](#). The absorption peak at 3437 cm^{-1} represents O-H tensile vibration, 1647 cm^{-1} belongs to O-H bending vibration, 1447 , 870 - 890 and 735 cm^{-1} are the vibration peaks of CO_3^{2-} in calcite and the characteristic peak of the C-S-H gel. The peak at 970 cm^{-1} relates to the asymmetric stretching of Si-O-T (T = Si/Al) in the N-A-S-H gel, while 665 cm^{-1} resulted from the Si-Al bending vibration of Si-O-Al in the N-A-S-H gel^[33]. The results suggest the formation of C-S-H and N-A-S-H gels in the reaction, which is consistent with the XRD results. In addition, compared to geopolymers exposed in air and freezing-thawing cycles, the peak at 1447 cm^{-1} of the geopolymers with 20% and 50% BFS exposed in the carbonization environment have larger adsorption intensity, which could be attributed to the invasion of CO_2 and the production of CO_3^{2-} . For the geopolymer with 20% BFS exposed to carbonization, the peak at 1447 cm^{-1} is obviously weakened. This is because in fly ash-slag polymer, the increase of FA can optimize the pore structure and reduce the pore size, resulting in less CO_2 ^[33]. Moreover, the FA activity is low and thus the unreacted FA particles can fill the holes in the geopolymer, thereby reducing the intrusion of CO_2 ^[33].

BET analysis

To obtain a clear understanding of the surface properties of the geopolymers prepared with different proportions of BFS in different exposure conditions, the BET test was used in the experiment to detect their specific surface areas and average pore sizes, as presented in [Figure 5](#) and listed in [Table 2](#). As can be seen in [Figure 5](#), all the geopolymers display similar adsorption-desorption curves, except the curve for the geopolymer with 100% BFS in freezing-thawing cycles, which was unconsolidated in the experiment. In the same environment (air or carbonization or freezing-thawing cycles), the BET surface area shows an increase and then decrease when increasing the BFS proportion, with the largest BET value found for the 50% BFS sample. However, the average pore sizes of these geopolymers are close and irregular. Moreover, the BET surface areas of the geopolymers exposed to carbonization environments always show greater values than those in air and freezing-thawing cycles, even though they display the smallest average pore size in the same BFS proportion. This could be attributed to the CaCO_3 not filling and blocking the pores but separating the larger pores into smaller pores. Thus, the BET surface area increases while the average pore size decreases to produce a richer porous structure. Thus, we can speculate that the geopolymers exposed to carbonization have the richest porous structures, which is significantly beneficial for improving the properties of geopolymers.

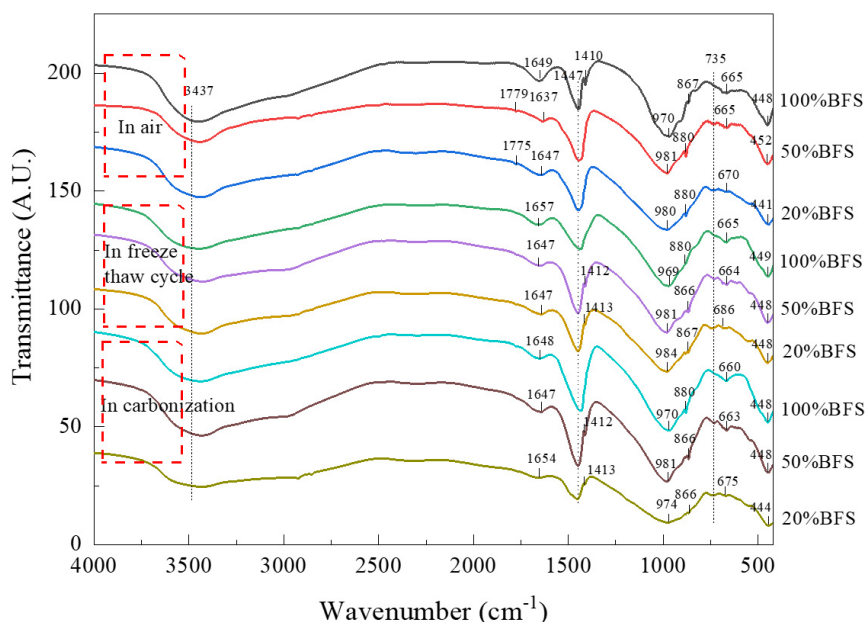
NMR analysis

To understand the nanostructural variations in the geopolymers exposed to different conditions, NMR spectroscopy was employed to detect their short-range ordering and molecular structure of the geopolymers

Table 2. BET surface areas and average pore sizes of geopolymers prepared with different proportions of BFS in different exposure conditions

Exposure condition	Samples	In air environment	In carbonization environment	In freezing-thawing cycles
BET surface area (m ² /g)	20% BFS	0.3950	1.5133	1.5802
	50% BFS	0.9090	1.8054	1.6250
	100% BFS	0.6100	1.0615	0.4858
Average pore size (μm)	20% BFS	25.64	19.44	19.48
	50% BFS	20.26	19.69	21.08
	100% BFS	22.66	20.23	24.51

BFS: Blast furnace slag.

**Figure 4.** FTIR spectra of geopolymers prepared with different proportions of BFS in different exposure conditions. BFS: Blast furnace slag.

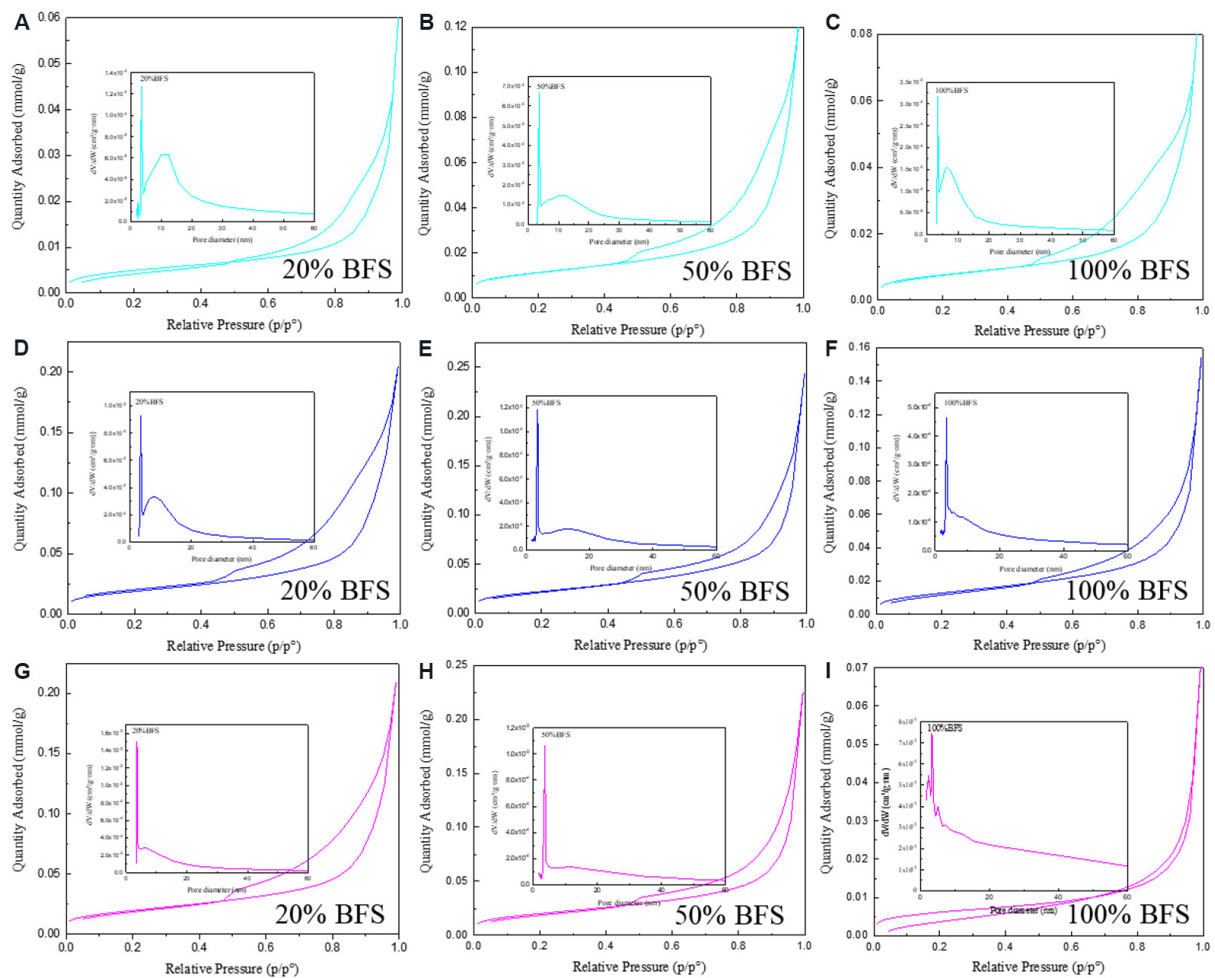
in Figure 6. It uses Gaussian peak deconvolution to overcome the lack of spectra resolution and can efficiently separate and quantify the $Q^n(mAl)$ species ($0 \leq m \leq n \leq 4$, m and n are integers)^[34,35]. The resonances at -74, -79, -87.8 and -96.4 ppm belong to Q^0 , Q^1 , Q^2 and Q^3 produced in the C-S-H gel, respectively^[36]. The resonances at -84, -89, -93, -99 and -108 ppm relate to $Q^4(4Al)$, $Q^4(3Al)$, $Q^4(2Al)$, $Q^4(1Al)$ and $Q^4(0Al)$ in the N-A-S-H gel, respectively^[37]. Furthermore, the resonance at -104 ppm represents $Q^3(R)$ when the H in OH is replaced by a metal ion (Na^+ or K^+) in Q^3 ^[38]. Figure 6 presents the ²⁹Si NMR spectra of geopolymers prepared with different proportions of BFS in different exposures. As can be seen, the ²⁹Si NMR spectra of the geopolymers exhibit a broad resonance ranging from δ_{iso} -75 to -95 ppm. However, the line shapes of the distribution are different, suggesting that various nanostructures occur in the geopolymers with different exposure conditions.

To further understand the nanostructural variations in the geopolymers under different exposures, the short-range ordering and molecular structure of the geopolymer were measured by NMR spectroscopy in Figure 7 and their corresponding Si sites are listed in Table 3. The 20%, 50% and 100% additions of BFS in

Table 3. Si sites in unreacted silicate resource and C-S-H and N-A-S-H gels

Exposure condition	Samples	Q ⁰ unreacted silicate	Q ¹ , Q ² , Q ³ (C-S-H)	Q ⁴ (N-A-S-H)
In air environment	20% BFS	2.55%	43.98%	53.47%
	50% BFS	5.64%	48.79%	45.57%
	100% BFS	16.91%	54.62%	28.47%
In carbonization environment	20% BFS	4.06%	48.76%	47.18%
	50% BFS	5.71%	39.78%	54.51%
	100% BFS	12.87%	51.46%	35.67%
In freezing-thawing cycles	20% BFS	2.72%	35.44%	61.84%
	50% BFS	6.85%	54.01%	39.14%
	100% BFS	11.86%	53.93%	34.21%

BFS: Blast furnace slag.

**Figure 5.** BET adsorption-desorption curves and pore size distribution of geopolymers prepared with different proportions of BFS in (A-C) air, (D-F) carbonization and (G-I) freezing-thawing cycles. BFS: Blast furnace slag.

the geopolymers are labeled low, medium and high calcium geopolymers, respectively. For the low calcium geopolymers exposed to air, carbonization and freezing-thawing cycles, their Si sites in the silicate monomers (Q⁰) are 2.55%, 4.06% and 2.72%, respectively, which display very low proportions and minimal

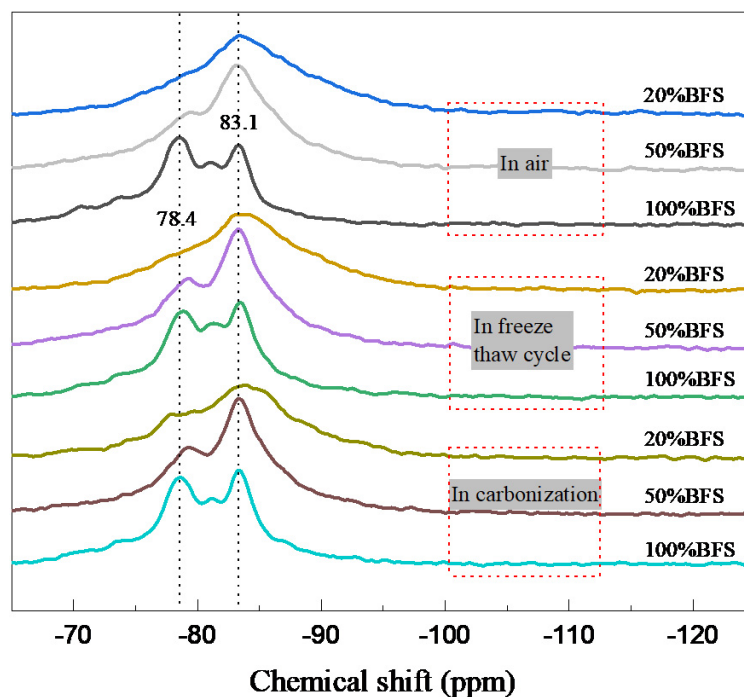


Figure 6. ^{29}Si NMR spectra of geopolymers prepared with different proportions of BFS in different exposure conditions. NMR: Nuclear magnetic resonance; BFS: blast furnace slag.

differences. These results suggest that most Si joined the geopolymerization reaction and the few unreacted Si may barely affect the geopolymer properties. Simultaneously, the Si sites Q^4 resulting from the N-A-S-H gel in the low calcium geopolymers under different exposure follows in carbonization (47.18%) < in air (53.47%) < in freezing-thawing cycles (61.84%), consistent with their compressive strength results in [Figure 2](#). Thus, we can speculate that the N-A-S-H gel conducts the properties of the low calcium geopolymer.

For the medium calcium geopolymers exposed to air, carbonization and freezing-thawing cycles, their Si sites in silicate monomers (Q^0) are 5.64%, 5.71% and 6.85%, respectively, which also display very low proportions and minimal differences. Meanwhile, the Si sites Q^1 , Q^2 and Q^3 resulting from the C-S-H gel in the medium calcium geopolymers under different exposure follows in carbonization (39.78%) < in air (48.79%) < in freezing-thawing cycles (54.01%), which also agrees with their compressive strengths. Thus, C-S-H gel may control the properties of the medium calcium geopolymers. For the high calcium geopolymers, it is difficult to conclude due to the collapse of geopolymer under freezing-thawing cycles. Although the high calcium geopolymers exposed in air contains more unreacted silicate Q^0 (16.91%) than that (12.87%) exposed to carbonization, the Si sites Q^1 , Q^2 and Q^3 in geopolymers exposed in air (54.62%) is higher as compared to that (51.46%) exposed to carbonization, consistent with their compressive strengths. These results suggest that the C-S-H gel dominates the properties of high calcium geopolymers.

Micromorphological analysis

For microobservation of the morphologies of the geopolymers prepared with different proportions of BFS in different exposures, [Figure 8](#) gives their typical SEM images. When exposed to air, only few unreacted particles can be observed, most of the raw materials reacted to produce geopolymer gels. In particular, more compact and smoother surfaces with increasing BFS addition are found, suggesting more geopolymer gel

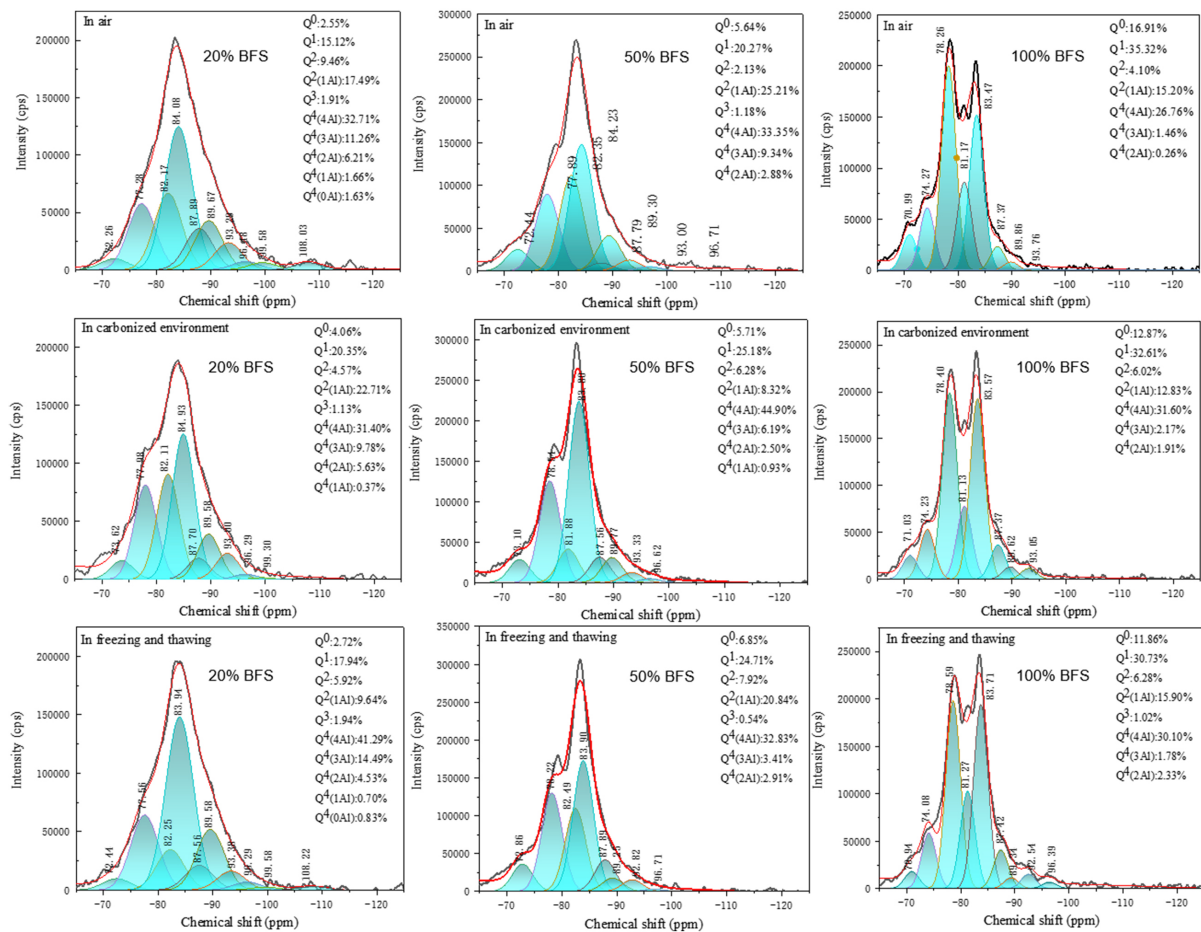


Figure 7. Deconvolution of ^{29}Si NMR spectra of geopolymers prepared with different proportions of BFS in (A-C) air, (D-F) carbonization and (G-I) freezing-thawing cycles. NMR: Nuclear magnetic resonance; BFS: blast furnace slag.

generation and better properties. While deeper and larger cracks occur with increasing BFS due to the natural evaporation of water, drying and shrinkage of sample, which may result in the surface tension increase larger than the binding force of geopolymers, which then cause some adverse effects on their properties.

When exposed to carbonization, the geopolymers with 20% and 50% BFS have fewer unreacted particles, smoother surface and smaller cracks when compared to that exposed in air, making them better properties, consistent with the compressive strength. Although the geopolymer with 100% BFS has smoother surface and smaller cracks, there are many unreacted particles on its surface, making it less compressive. These results can be attributed to the FA optimizing the pore structure of the fly ash-slag base polymer, effectively preventing carbon dioxide from entering the interior and reducing the negative effects brought by the neutralization of pore fluid and the generation of CaCO_3 and other expansive substances caused by carbon dioxide.

For exposure to freezing-thawing cycles, the sample under 20% BFS has significantly fewer unreacted particles and a more dense surface with some cracks, which is because FA optimizes the pore structure of fly ash-slag base polymer, effectively reducing seawater entry into the internal structure and performs better in freezing-thawing resistance^[39]. With increasing BFS, the geopolymer surface change to rough and occur

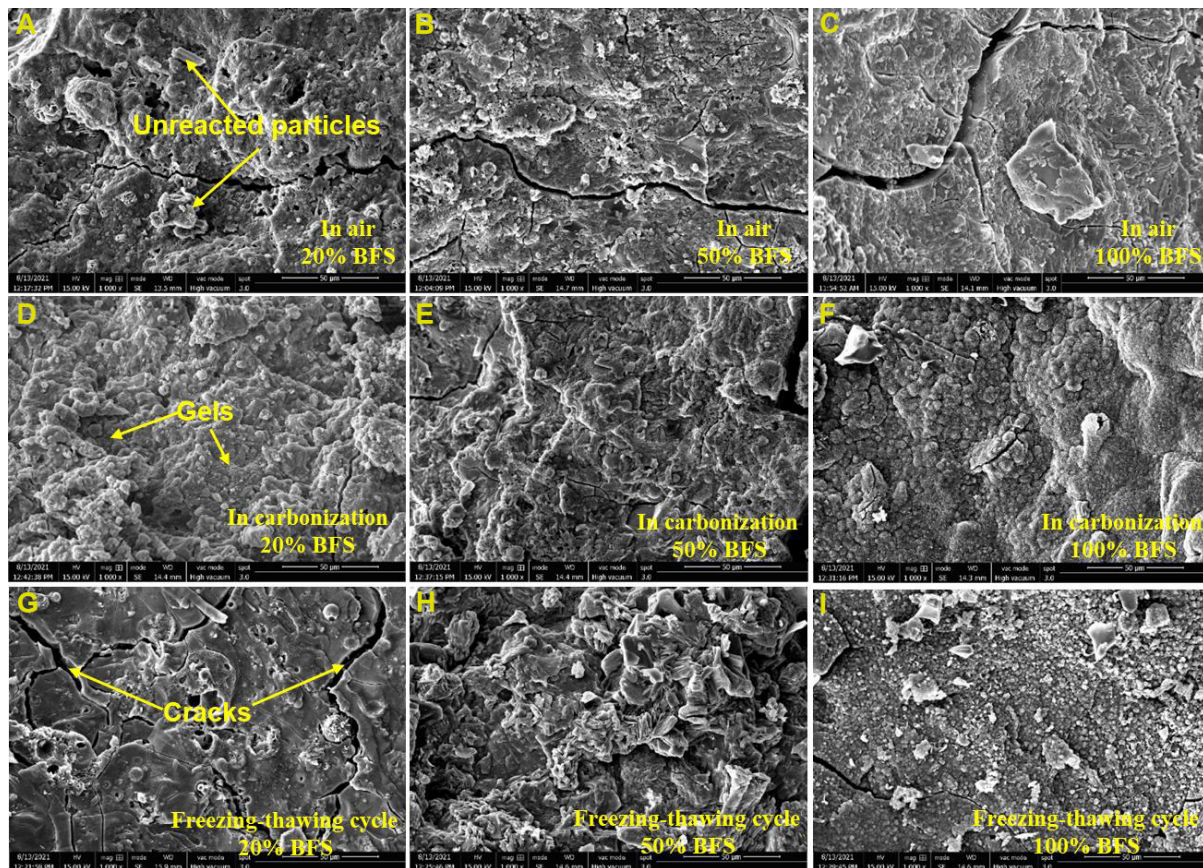


Figure 8. SEM images of geopolymers prepared with different proportions of BFS in (A-C) air, (D-F) carbonization and (G-I) freezing-thawing cycles. SEM: Scanning electron microscopy; BFS: blast furnace slag.

many unreacted particles. Compared with in carbonization, the harm caused by freeze-thaw cycles is far more than that of carbonization and the late hydration cannot be carried out because of overall cracking.

Macromorphology exposed in freezing-thawing cycles

Based on the above results, the geopolymers exposed to freezing-thawing cycles encounter the most severe deterioration. To obtain a visual observation of the process, [Figure 9](#) gives the macro changes of the geopolymer prepared with different proportions of BFS in freezing-thawing cycles. It can be seen that all the initial geopolymers show a strong cubic shape in the 10%-100% proportion range of BFS. However, the geopolymers with 60%-100% BFS display an unconsolidated matrix after ten freezing-thawing cycles. Therefore, it is failed to obtain the compressive strength value of geopolymer with 60%-100% BFS. As the samples encounter 20 freezing-thawing cycles, almost all the geopolymers present an unconsolidated matrix and the more BFS, the more severe the unconsolidation. The NMR analysis finds that geopolymers exposed to freezing-thawing cycle are of fewer Si sites in Q^0 while much more Si sites in Q^1 , Q^2 , Q^3 and Q^4 , which has a similar evolution trend to those of geopolymers exposed in air and carbonization. Geopolymers exposed to air and carbonization exhibit higher compressive strength than that exposed in freezing-thawing cycles. In contrast, the geopolymers exposed to freezing-thawing cycles exhibit the most severe deterioration. This result indicates that the deterioration is not related to the evolution of chemical nanostructures but with the changes in physical properties. The formation of the cracks caused by the fast drying and shrinkage of geopolymer, which might result in the deterioration of geopolymers. In the freezing-thawing cycles, water saturating, freezing, swelling and melting in cracks take place reduplicative, thus accelerating the

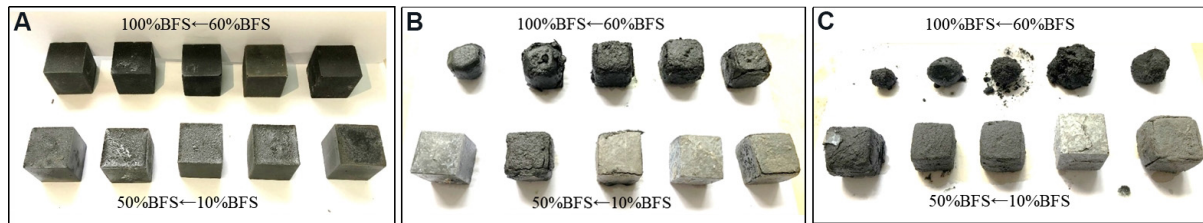


Figure 9. Macro changes of geopolymers prepared with different proportions of BFS in freezing-thawing cycles for (A) initial sample, (B) 10 times and (C) 20 times. BFS: Blast furnace slag.

decomposition of the geopolymer matrix.

CONCLUSION

The present work investigated the role of calcium in BFS-FA geopolymers under various artificial natural environments. It was found that two kinds of geopolymer gels, C-S-H and N-A-S-H, occurred in the geopolymerization of BFS and FA. In the low calcium geopolymer, the N-A-S-H gel dominates its properties regardless of the geopolymer environment. While in the medium and high calcium geopolymers, the C-S-H gel conducts the properties regardless of the environments. In addition, the geopolymer exposed in carbonization possesses higher surface area and smaller pore size, suggesting the geopolymer has a richer pore structure, which is significantly beneficial for improving its properties.

DECLARATIONS

Authors' contributions

Substantial contributions to conception and design of the study: Rao F, Liu W, Ma H

Performed data acquisition and data analysis: Li J

performed data interpretation and wrote the manuscript: Yang L

Provided administrative, technical, and material support: Chi X, Zhong S

Availability of data and materials

Not applicable.

Financial support and sponsorship

This study was financially supported by the National Natural Science Foundation of China (Project No. 51974093) and the Minjiang Scholar Talent Foundation of Fujian Province (Grant No. GXRC-20067), for which the authors are grateful.

Conflicts of interest

All authors declared that there are no conflicts of interest.

Ethical approval and consent to participate

Not applicable.

Consent for publication

Not applicable.

Copyright

© The Author(s) 2022.

REFERENCES

1. Davidovits J. Geopolymer cement. A review. Geopolymer institute. *Tech Pap* 2013;21:1-11.
2. Davidovits J. Global warming impact on the cement and aggregates industries. *World Resour Rev* 1994;6:263-78. DOI
3. Yusuf MO, Johari MAM, Ahmad ZA, Maslehuddin M. Strength and microstructure of alkali-activated binary blended binder containing palm oil fuel ash and ground blast-furnace slag. *Constr Build Mater* 2014;52:504-10. DOI
4. Part WK, Ramli M, Cheah CB. An overview on the influence of various factors on the properties of geopolymer concrete derived from industrial by-products. *Constr Build Mater* 2015;77:370-95. DOI
5. Aiken TA, Kwasny J, Sha W, Soutsos MN. Effect of slag content and activator dosage on the resistance of fly ash geopolymer binders to sulfuric acid attack. *Cem Concr Res* 2018;111:23-40. DOI
6. García de Arquer FP, Bushuyev OS, De Luna P, et al. 2D metal oxyhalide-derived catalysts for efficient CO₂ electroreduction. *Adv Mater* 2018;30:1802858. DOI PubMed
7. Vinai R, Rafeet A, Soutsos M, Sha W. The role of water content and paste proportion on physico-mechanical properties of alkali activated fly ash-ggbs concrete. *J Sustain Metall* 2016;2:51-61. DOI
8. Zhang Z, Provis JL, Reid A, Wang H. Geopolymer foam concrete: an emerging material for sustainable construction. *Constr Build Mater* 2014;56:113-27. DOI
9. Davidovits J. Geopolymers and geopolymeric materials. *J Therm Anal* 1989;35:429-41. DOI
10. Thokchom S, Ghosh P, Ghosh S. Performance of fly ash based geopolymer mortars in sulphate solution. *J Eng Sci Technol Rev* 2010;3:36-40. DOI
11. Rangan BV. Geopolymer concrete for environmental protection. *Indian Concr J* 2014;88:41-59. DOI
12. Crozier DA, Sanjayan JG. Chemical and physical degradation of concrete at elevated temperatures. *Concr Aust* 1999. DOI
13. Rovnanik P. Effect of curing temperature on the development of hard structure of metakaolin-based geopolymer. *Constr Build Mater* 2010;24:1176-83. DOI
14. Prud'Homme E, Michaud P, Joussein E, Peyratout C, Smith A, Rossignol S. In situ inorganic foams prepared from various clays at low temperature. *Appl Clay Sci* 2011;51:15-22. DOI
15. He J, Zhang J, Yu Y, Zhang G. The strength and microstructure of two geopolymers derived from metakaolin and red mud-fly ash admixture: a comparative study. *Constr Build Mater* 2012;30:80-91. DOI
16. Tho-in T, Sata V, Chindaprasirt P, Jaturapitakkul C. Pervious high-calcium fly ash geopolymer concrete. *Constr Build Mater* 2012;30:366-71. DOI
17. Rickard WDA, Temuujin J, van Riessen A. Thermal analysis of geopolymer pastes synthesised from five fly ashes of variable composition. *J Non Cryst Solids* 2012;358:1830-9. DOI
18. Ahmari S, Zhang L. Production of eco-friendly bricks from copper mine tailings through geopolymerization. *Constr Build Mater* 2012;29:323-31. DOI
19. Zhuguo LI, Sha L. Carbonation resistance of fly ash and blast furnace slag based geopolymer concrete. *Constr Build Mater* 2018;163:668-80. DOI
20. Xu H, Gong W, Syltebo L, Izzo K, Lutze W, Pegg IL. Effect of blast furnace slag grades on fly ash based geopolymer waste forms. *Fuel* 2014;133:332-40. DOI
21. Kumar S, Kumar R, Mehrotra SP. Influence of granulated blast furnace slag on the reaction, structure and properties of fly ash based geopolymer. *J Mater Sci* 2010;45:607-15. DOI
22. Kumar S, Vasugi J, Ambily PS, Bharatkumar BH. Development and determination of mechanical properties of fly ash and slag blended geopolymer concrete. *Int J Sci Eng Res* 2013. DOI
23. Nath P, Sarker PK. Effect of GGBFS on setting, workability and early strength properties of fly ash geopolymer concrete cured in ambient condition. *Constr Build Mater* 2014;66:163-71. DOI
24. Lloyd RR, Provis JL, van Deventer JSJ. Microscopy and microanalysis of inorganic polymer cements. 2: the gel binder. *J Mater Sci* 2009;44:620-31. DOI
25. Temuujin J V, Van Riessen A, Williams R. Influence of calcium compounds on the mechanical properties of fly ash geopolymer pastes. *J Hazard Mater* 2009;167:82-8. DOI PubMed
26. Yip CK, van Deventer JSJ. Microanalysis of calcium silicate hydrate gel formed within a geopolymeric binder. *J Mater Sci* 2003;38:3851-60. DOI
27. Yip CK, Lukey GC, Provis JL, van Deventer JSJ. Effect of calcium silicate sources on geopolymerisation. *Cem Concr Res* 2008;38:554-64. DOI
28. Garcia-Lodeiro I, Palomo A, Fernández-Jiménez A, Macphee DE. Compatibility studies between N-A-S-H and C-A-S-H gels. Study in the ternary diagram Na₂O-CaO-Al₂O₃-SiO₂-H₂O. *Cem Concr Res* 2011;41:923-31. DOI
29. Khan MSH, Castel A, Akbarnezhad A, Foster SJ, Smith M. Utilisation of steel furnace slag coarse aggregate in a low calcium fly ash geopolymer concrete. *Cem Concr Res* 2016;89:220-9. DOI
30. Phummiphon I, Horpibulsuk S, Rachan R, Arulrajah A, Shen SL, Chindaprasirt P. High calcium fly ash geopolymer stabilized lateritic soil and granulated blast furnace slag blends as a pavement base material. *J Hazard Mater* 2018;341:257-67. DOI PubMed
31. Xu J, Kang A, Wu Z, Xiao P, Gong Y. Effect of high-calcium basalt fiber on the workability, mechanical properties and microstructure of slag-fly ash geopolymer grouting material. *Constr Build Mater* 2021;302:124089. DOI
32. Torres JJ, Palacios M, Hellouin M, Puertas F. Alkaline chemical activation of urban glass wastes to produce cementitious materials. 1st Spanish Natl Conf Adv Mater Recycl Eco-Energy; 2009 Nov 12-13; Madrid, Spain. 2009. p.111-4.

33. Tian X, Rao F, León-Patiño CA, Song S. Co-disposal of MSWI fly ash and spent caustic through alkaline-activation consolidation. *Cem Concr Compos* 2021;116:103888. [DOI](#)
34. Klinowski J. Nuclear magnetic resonance studies of zeolites. *Prog Nucl Magn Reson Spectrosc* 1984;16:237-309. [DOI](#) [PubMed](#)
35. Tian X, Rao F, Morales-Estrella R, Song S. Effects of aluminum dosage on gel formation and heavy metal immobilization in alkali-activated municipal solid waste incineration fly ash. *Energy & Fuels* 2020;34:4727-33. [DOI](#)
36. Singh PS, Bastow T, Trigg M. Structural studies of geopolymers by ²⁹Si and ²⁷Al MAS-NMR. *J Mater Sci* 2005;40:3951-61. [DOI](#)
37. Engelhardt G, Michel D. High-resolution solid-state NMR of silicates and zeolites. *Applied Catalysis* 1987;42:187-8. [DOI](#)
38. Tian X, Xu W, Song S, Rao F, Xia L. Effects of curing temperature on the compressive strength and microstructure of copper tailing-based geopolymers. *Chemosphere* 2020;253:126754. [DOI](#) [PubMed](#)
39. Li S, Peng XQ, Gou Q. Effect of mineral admixtures on frost resistance of geopolymers. *Mater Rev* 2018;32:1711-5. [DOI](#)